Fibroblast-derived CSF1 maintains colonization of gut mucosal macrophage to resist bacterial infection

Nonaka, Daichi
Division of Mucosal Immunology, Medical Institute of Bioregulation, Kyushu University

Yoshida, Soichiro
Division of Mucosal Immunology, Medical Institute of Bioregulation, Kyushu University

Nakano, Kenta
Department of Laboratory Animal Medicine, Research Institute, National Center for Global Health and Medicine (NCGM)

Li, Xiaojun
Division of Mucosal Immunology, Medical Institute of Bioregulation, Kyushu University

他

出版情報：Mucosal Immunology. 18 (5), pp.1113-1123, 2025-10-08. Elsevier
バージョン：

Mucosal Immunology xxx (xxxx) xxx

Contents lists available at ScienceDirect

Mucosal Immunology

journal homepage: www.elsevier.com/mi

Fibroblast-derived CSF1 maintains colonization of gut mucosal macrophage to resist bacterial infection

Daichi Nonaka [a,2], Soichiro Yoshida [a,2], Kenta Nakano [b], Xiaojun Li [a,c], Tadashi Okamura [b], Eiji Umemoto [d], Taisho Yamada [a], Miyuki Watanabe [a], Shozo Jinno [e], Minako Ito [f], Makoto Tsuda [g], Naoto Noguchi [a], Jean X Jiang [h], Eriko Sumiya [a,3,4], Shinichiro Sawa [a,1,3,*]

[a] Division of Mucosal Immunology, Medical Institute of Bioregulation, Kyushu University, Fukuoka 812-8582, Japan
[b] Department of Laboratory Animal Medicine, Research Institute, National Center for Global Health and Medicine (NCGM), Tokyo 162-8655, Japan
[c] The Second Xiangya Hospital of Central South University, department of gastroenterology, Changsha, Hunan 410000, China
[d] Laboratory of Microbiology and Immunology, School of Pharmaceutical Sciences, University of Shizuoka, Shizuoka 422-8526, Japan
[e] Department of Anatomy and Neuroscience, Graduate School of Medical Sciences, Kyushu University, Fukuoka 812-8582, Japan
[f] Division of Allergy and Immunology, Medical Institute of Bioregulation, Kyushu University, Fukuoka 812-8582, Japan
[g] Department of Molecular and System Pharmacology, Graduate School of Pharmaceutical Sciences, Kyushu University, Fukuoka 812-8582, Japan
[h] Department of Biochemistry and Structural Biology, University of Texas Health Science Center, San Antonio, TX 78229-3900, USA

ARTICLE INFO

Keywords:
Macrophage
Niche
CSF1
IL-34
Fibroblast
Intestine

ABSTRACT

Macrophages play essential roles in immune defense and tissue homeostasis, but the mechanisms underlying their colonization in the gut mucosa remain incompletely understood. Here, we identify CSF1, primarily derived from fibroblasts, as the dominant factor maintaining mucosal macrophage colonization, whereas IL-34 deficiency alone has a minimal impact. We reveal that CSF1R ligands originate from distinct cellular sources: macrophages at the upper villus region depend on fibroblast-derived CSF1 and IL-34, while macrophages in the lower villus and the submucosal (lower villus + SM) region are regulated by CSF1 from both fibroblasts and endothelial cells. Additionally, within the lower villus + SM region, CSF1-producing CD81^{+} LepR^{+} fibroblasts directly interact with CD163^{+} macrophages, forming a localized niche. The loss of CSF1 in fibroblasts results in accelerated systemic dissemination of *Salmonella* Typhimurium, highlighting fibroblast-derived CSF1 as a key regulator of gut macrophage function in host defense. Collectively, our findings uncover a previously unrecognized fibroblast-macrophage crosstalk that governs gut macrophage homeostasis and immunity.

Introduction

Macrophages, a major component of the mononuclear phagocyte system, are present in most vertebrate tissues, where they contribute to immunity, development, metabolic homeostasis, and tissue repair[1–3]. During embryogenesis, yolk sac erythro-myeloid progenitors generate pre-macrophages and monocytes, which colonize developing tissues and differentiate into tissue-resident macrophages, maintaining their populations locally throughout life[4]. Postnatally, bone marrow (BM)-derived monocytes can replenish certain macrophage pools, particularly under inflammatory conditions[5,6].

The intestine performs multiple functions, including nutrient absorption, immune surveillance, and tolerance to dietary and commensal antigens[7]. Gut-resident macrophages, located primarily in the lamina propria, play a pivotal role in maintaining gut homeostasis by sampling luminal contents through dendritic projections and initiating immune responses against pathogenic microbes via pattern recognition receptors[8–10]. Additionally, they regulate both innate and adaptive

* Corresponding author at: Division of Mucosal Immunology, Medical Institute of Bioregulation, Kyushu University, Fukuoka, 812-8582, Japan.
E-mail address: sawa@bioreg.kyushu-u.ac.jp (S. Sawa).
[1] Lead contact.
[2] Daichi Nonaka and Soichiro Yoshida Contributed equally to this work and share first authorship.
[3] Eriko Sumiya and Shinichiro Sawa Contributed equally to this work and share last authorship.
[4] Present address: Department of Orthopedic Surgery, Faculty of Medicine, University of Tokyo, Tokyo, 113-0033, Japan.

https://doi.org/10.1016/j.mucimm.2025.06.011
Received 6 August 2024; Accepted 30 June 2025
Available online 1 July 2025

immune responses to amplify host defense mechanisms[11–13]. Importantly, gut macrophages also exhibit immunoregulatory functions, such as clearing apoptotic cells and producing IL-10, an anti-inflammatory cytokine critical for suppressing excessive immune activation[14,15]. Dysfunction in these regulatory pathways has been implicated in inflammatory bowel diseases (IBD)[16].

Anatomically, the intestine consists of two major compartments: the mucosa and the muscularis externa. The mucosa includes the epithelial layer, lamina propria (LP) and submucosa. In some contexts, the LP and submucosa are collectively considered and further subdivided into the upper and the lower LP zones[17]. The role of gut resident macrophages is considered to be specialized in a region-specific manner[18]. Lamina propria macrophages, positioned just beneath the epithelium, play an integral role in antigen sampling and immune homeostasis. Beyond their immune functions, gut macrophages contribute to intestinal architecture, including vascular homeostasis[19]. In the crypt-lower villus compartment, macrophages near crypt regions support Lgr5^{+} intestinal epithelial stem cells via Wnt signaling, particularly during homeostasis and tissue repair following injury[20,21]. Tissue-specific factors are increasingly recognized as key determinants of macrophage identity and

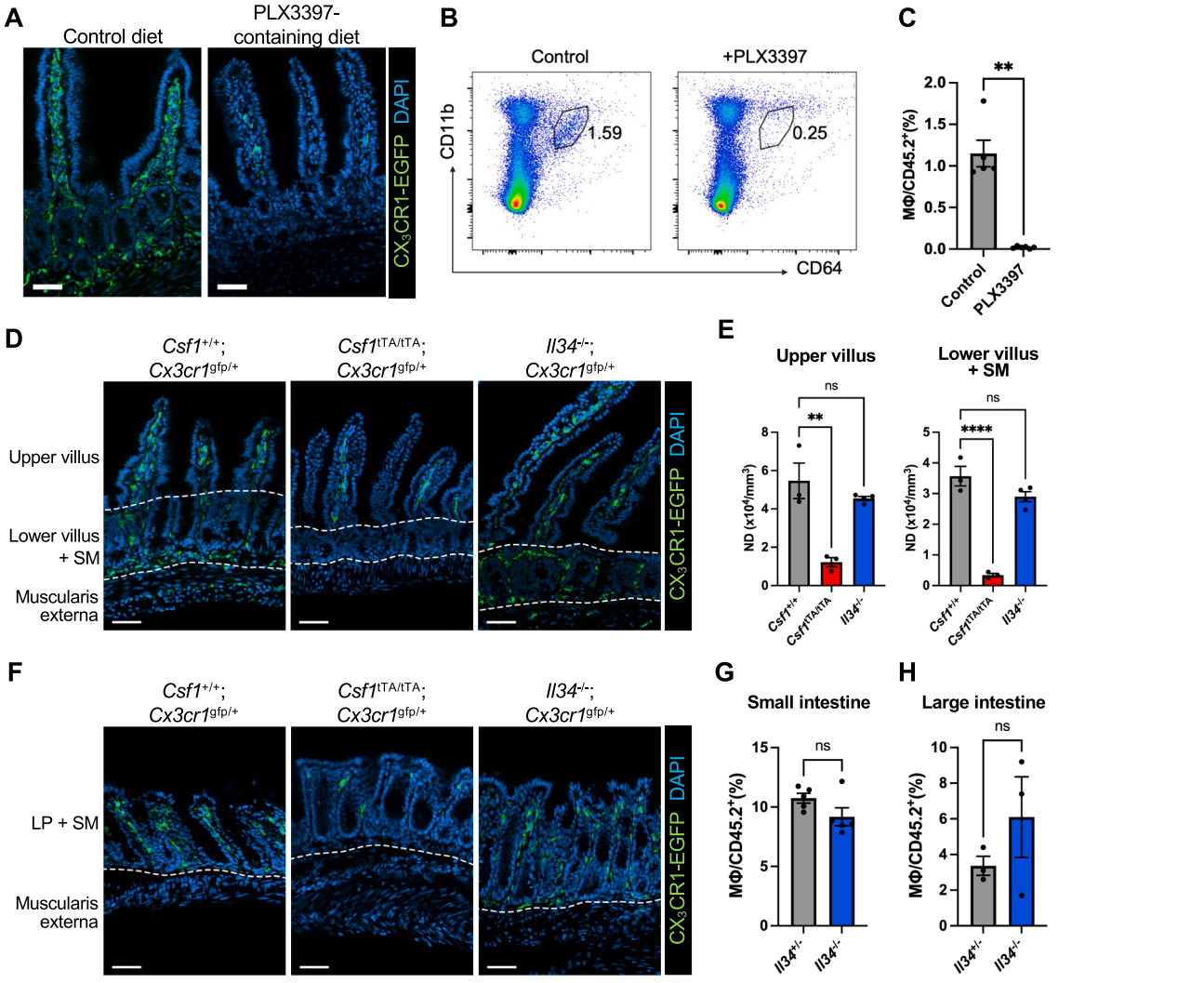

Fig. 1. CSF1 is predominantly required for gut mucosal macrophage pool. (A) Representative confocal microscopy images of the jejunum from 9-week-old *Cx3cr1*$^{gfp/+}$ mice fed either a normal diet or a PLX3397-containing diet for 2 weeks. Macrophages and nuclei are visualized by CX_3CR1-EGFP and DAPI, respectively. Scale bars, 50 μm. (B) Flow cytometry analysis of small intestinal macrophages from 9-week-old *Cx3cr1*$^{gfp/+}$ mice on the indicated diets. Representative expression patterns of CD11b and CD64 among live CD45.2^{+} small intestinal cells are shown. Numbers indicate the percentages of gated populations. (C) Quantification of macrophages in the small intestine from (B). Data represent *Cx3cr1*$^{gfp/+}$ mice fed a normal (n = 5) or PLX3397-containing diet (n = 6). The experiment was performed twice. (D) Representative confocal microscopy images of the jejunum from 4-week-old *Csf1*$^{+/+}$ *Cx3cr1*$^{gfp/+}$, *Csf1*$^{tTA/tTA}$; *Cx3cr1*$^{gfp/+}$ and *Il34*$^{-/-}$; *Cx3cr1*$^{gfp/+}$ mice. Macrophages and nuclei are labeled with CX_3CR1-EGFP and DAPI. Dashed lines indicate boundaries of the upper villus, lower villus + submucosa (SM), and muscularis externa. Scale bars, 50 μm. (E) Quantification of macrophages in the upper villus and lower villus + SM regions from (D). Data represent *Csf1*$^{+/+}$; *Cx3cr1*$^{gfp/+}$ (n = 3), *Csf1*$^{tTA/tTA}$; *Cx3cr1*$^{gfp/+}$ (n = 3), and *Il34*$^{-/-}$; *Cx3cr1*$^{gfp/+}$ (n = 4) mice. The experiment was performed twice for *Csf1*$^{tTA/tTA}$ and three times for *Il34*$^{-/-}$ mice. (F) Representative confocal images of the distal large intestine from 4-week-old *Csf1*$^{+/+}$; *Cx3cr1*$^{gfp/+}$, *Csf1*$^{tTA/tTA}$; *Cx3cr1*$^{gfp/+}$ and *Il34*$^{-/-}$; *Cx3cr1*$^{gfp/+}$ mice. Macrophages and nuclei are visualized with CX_3CR1-EGFP and DAPI. Dashed lines indicate the boundary between the lamina propria (LP) + submucosa and the muscularis externa. Scale bars, 50 μm. The experiment was repeated three times. (G) Flow cytometry analysis of small intestinal macrophages in 4-week-old *Il34*$^{+/-}$ (n = 5) and *Il34*$^{-/-}$(n = 5) mice. Frequencies of CD11b^{+} CD64^{+} Ly6C^{low} MHCII^{high} cells among CD45.2^{+} cells are shown. The experiment was performed three times. (H) Flow cytometry analysis of large intestinal macrophages in 4-week-old *Il34*$^{+/-}$ (n = 3) and *Il34*$^{-/-}$ (n = 3) mice. Frequencies of CD11b^{+} CD64^{+} Ly6C^{low} MHCII^{high} cells among CD45.2^{+} cells are shown. The experiment was performed twice. Data are pooled from at least two independent experiments and presented as mean ± SEM. Statistical analyses were performed using the unpaired Mann-Whitney test (C), one-way ANOVA with Dunnett's multiple comparison test (E), and unpaired *t*-test (F and H). Statistical significance is indicated as $^{**}p < 0.01$, $^{***}p < 0.001$, $^{****}p < 0.0001$; ns, not significant.

function[22,23]. In line with this, gut-resident macrophages exhibit highly heterogeneous transcriptomic profiles, suggesting that they integrate local environmental cues to acquire distinct functional phenotypes[24,25]. However, the mechanisms regulating the development, survival, and function of these macrophage subsets remain poorly understood.

Like other leukocytes, macrophages rely on extrinsic niche signals for their maintenance. Among these, Colony-Stimulating Factor 1 Receptor (CSF1R) signaling—mediated by its two cognate ligands, CSF1 and IL-34—is essential for macrophage proliferation, differentiation, and survival[26–28]. Mice lacking functional CSF1R exhibit a profound loss of macrophages across multiple tissues, resulting in severe defects such as impaired bone marrow cavity formation and defective brain myelination[29,30]. Although CSF1R ligands have been established as key macrophage niche factors in the intestine, their precise identity and specific cellular sources remain unknown[31].

In this study, we aimed to identify the cellular sources of CSF1R ligands within distinct intestinal compartments and elucidate their role in gut macrophage homeostasis. Using transcriptomic analysis combined with genetic models for cell lineage-specific depletion of CSF1R ligands, we identified podoplanin (PDPN)$^+$ fibroblasts as the primary source of CSF1, which was indispensable for sustaining gut mucosal macrophages. Furthermore, fibroblast-derived CSF1 played a critical role in host defense against *Salmonella* Typhimurium (*S*. Typhimurium) infection. These findings reveal an essential fibroblast-macrophage crosstalk that regulates gut macrophage homeostasis and host immunity, highlighting intestinal fibroblasts as key niche cells for maintaining the macrophage pool.

Results

CSF1 is predominantly required for the colonization of gut mucosal macrophages

We first confirmed the significance of the CSF1R signal in gut-resident macrophage. To this end, we examined the effect of CSF1R blockade in adult mice using *Cx3cr1*$^{gfp/+}$ reporter mice[32] (Supplementary Fig. 1A, B). Pexidartinib (PLX3397) is a potent multi-targeted inhibitor of receptor tyrosine kinases, including CSF1R[33]. Mice fed a PLX3397-containing diet for two weeks exhibited a complete depletion of CX3CR1-EGFP$^+$ macrophages in the intestine (Fig. 1A–C), indicating that CSF1R signaling is essential for the maintenance of gut macrophages.

CSF1 and IL-34 are cognate ligands for CSF1R in both mice and humans. To investigate the role of CSF1 in intestinal macrophage maintenance, we performed a histological analysis of small intestinal macrophages in four-week-old *Csf1*-deficient *Csf1*$^{tTA/tTA}$ mice (Supplementary Fig. 2A). Anatomically, we divided the small intestinal lamina propria into two regions: the upper villus and the crypt-lower villus regions referring to the previous report[17]. Because the submucosal (SM) layer in mice is too thin to be clearly distinguished from the crypt-lower villus regions, we defined the lamina propria excluding the upper villus as “lower villus”. Thus, the non-muscularis externa region of the small intestine was categorized into two compartments: “upper villus” and “lower villus + SM”. Similarly, we defined the non-muscularis externa region in the large intestine as the “lamina propria and SM region (LP + SM)”.

We observed a significant reduction of macrophages within the upper villus and lower villus + SM regions of the small intestine in *Csf1*$^{tTA/tTA}$ mice (Fig. 1D, E). This phenotype closely resembles that of *Csf1*$^{op/op}$ mice, which lack functional CSF1[34]. A similar trend was confirmed in the large intestine (Fig. 1F). In contrast, the number of mucosal macrophages in *Il34*$^{-/-}$ mice (Supplementary Fig. 2B–D) was comparable to that of control mice in the small intestine (Fig. 1D, E). Flow cytometry analysis further revealed no significant reduction in macrophages in either the small or large intestine of *Il34*$^{-/-}$ mice (Fig. 1G, H).

These data indicate that systemic loss of CSF1 severely impairs the colonization of gut mucosal macrophages, whereas IL-34 deficiency has no apparent impact on the macrophage pool. Therefore, we conclude that CSF1 is predominantly required for the colonization of gut mucosal macrophages.

PDPN$^+$ fibroblasts are major producers of CSF1 in the gut mucosa

Through alternative splicing and distinct proteolytic processing, CSF1 is produced in three isoforms: a secreted soluble form CSF1 (sCSF1), a secreted chondroitin sulfate form, and a cell-surface form[35]. Given that transgenic sCSF1 fails to compensate for endogenous CSF1 deficiency[36], we hypothesized that CSF1 is not uniformly distributed across gut regions and that macrophages are primarily maintained by locally provided CSF1[31]. To identify CSF1-producing cells in the gut, we generated *Csf1*$^{tTA/+}$; *LC1*; *Rosa26*$^{LSL\text{-}tdTomato}$ mice, which enable continuous labeling of *Csf1*-expressing cells and allow doxycycline (Dox)-regulated Cre expression[37,38]. Specifically, tTA expression is driven by the *Csf1* promoter, which activates Cre expression via binding to the tetracycline response element (TRE). Dox inhibits tTA binding to TRE, thereby preventing the labeling of cells with tdTomato (Supplementary Fig. 3A, B).

Flow cytometry analysis of lamina propria cells isolated from *Csf1*$^{tTA/+}$; *LC1*; *Rosa26*$^{LSL\text{-}tdTomato}$ mice revealed that the majority of cells with a history of *Csf1* expression were CD45$^-$ non-hematopoietic cells, particularly CD31$^-$ non-endothelial cells (Fig. 2A). Among them, PDPN$^+$ and PDPN$^-$ PDGFRα$^+$ fibroblasts selectively expressed tdTomato (Supplementary Fig. 3C). Histological analysis showed that *Csf1*fate-mapped cells were closely adjacent to CX3CR1-EGFP$^+$ macrophages in both the small and large intestines (Fig. 2B). Under Dox-free conditions, tdTomato expression was detected in upper villus PDPN$^+$ fibroblasts at both E15.5 and P1 (Fig. 2C). In addition, when Dox was withdrawn at 3 weeks of age, PDPN$^+$ fibroblasts in the upper villus region express tdTomato by 6 weeks after birth (Fig. 2C). *Csf1*fate-mapped cells in the villi co-immunostained with an anti-Cre antibody, confirming *Csf1* promoter activity in these cells (Fig. 2D). In the lower villus + SM region of *Csf1*$^{tTA/+}$; *LC1*; *Rosa26*$^{LSL\text{-}tdTomato}$ mice, tdTomato signals were detected in mesenchymal cells, including CD31$^+$ endothelial cells and PDPN$^+$ fibroblasts by 6 weeks of age, following Dox withdrawal at 3 weeks (Fig. 2E). Under the same condition, PDPN$^+$ fibroblasts were labeled with tdTomato in the large intestine (Fig. 2F). These data indicate that the *Csf1* promoter is active in mesenchymal cells within the lamina propria. The anatomical proximity between CX3CR1-EGFP$^+$ macrophages and tdTomato$^+$ mesenchymal cells strongly suggests tight cell–cell communication through local CSF1-dependent cues.

In parallel, we analyzed *Csf1* transcription among intestinal cells. *Csf1* mRNA levels were significantly higher in PDPN$^+$ fibroblasts than in CD45$^+$ hematopoietic cells and CD31$^+$ endothelial cells in both the small and large intestines (Fig. 3A, B). Notably, PDPN$^-$ CD31$^-$ fraction, which includes PDPN$^-$ PDGFRα$^+$ fibroblasts (Supplementary Fig. 3C), exhibited relatively lower *Csf1* mRNA expression than PDPN$^+$ fibroblasts and CD31$^+$ endothelial cells. Fate-mapping analysis using *Csf1*$^{tTA/+}$; *LC1*; *Rosa26*$^{LSL\text{-}tdTomato}$ mice confirmed that PDGFRα$^+$ fibroblasts, most of which are PDPN$^+$, are the major source of CSF1 (Supplementary Fig. 3C).

Intestinal fibroblast subpopulations uniformly express CSF1

Recent studies indicate that intestinal fibroblasts are highly heterogeneous, with distinct subpopulations exhibiting unique localization patterns[39–43]. To identify the specific fibroblast subsets that produce CSF1, we sorted PDPN$^+$ fibroblasts from the small intestinal lamina propria of wild-type mice and performed droplet-based single-cell RNA sequencing (scRNA-seq). Based on differentially expressed gene (DEG) profiles, PDPN$^+$ fibroblasts were classified into five clusters, which were annotated using marker gene expression and DEG-based comparisons

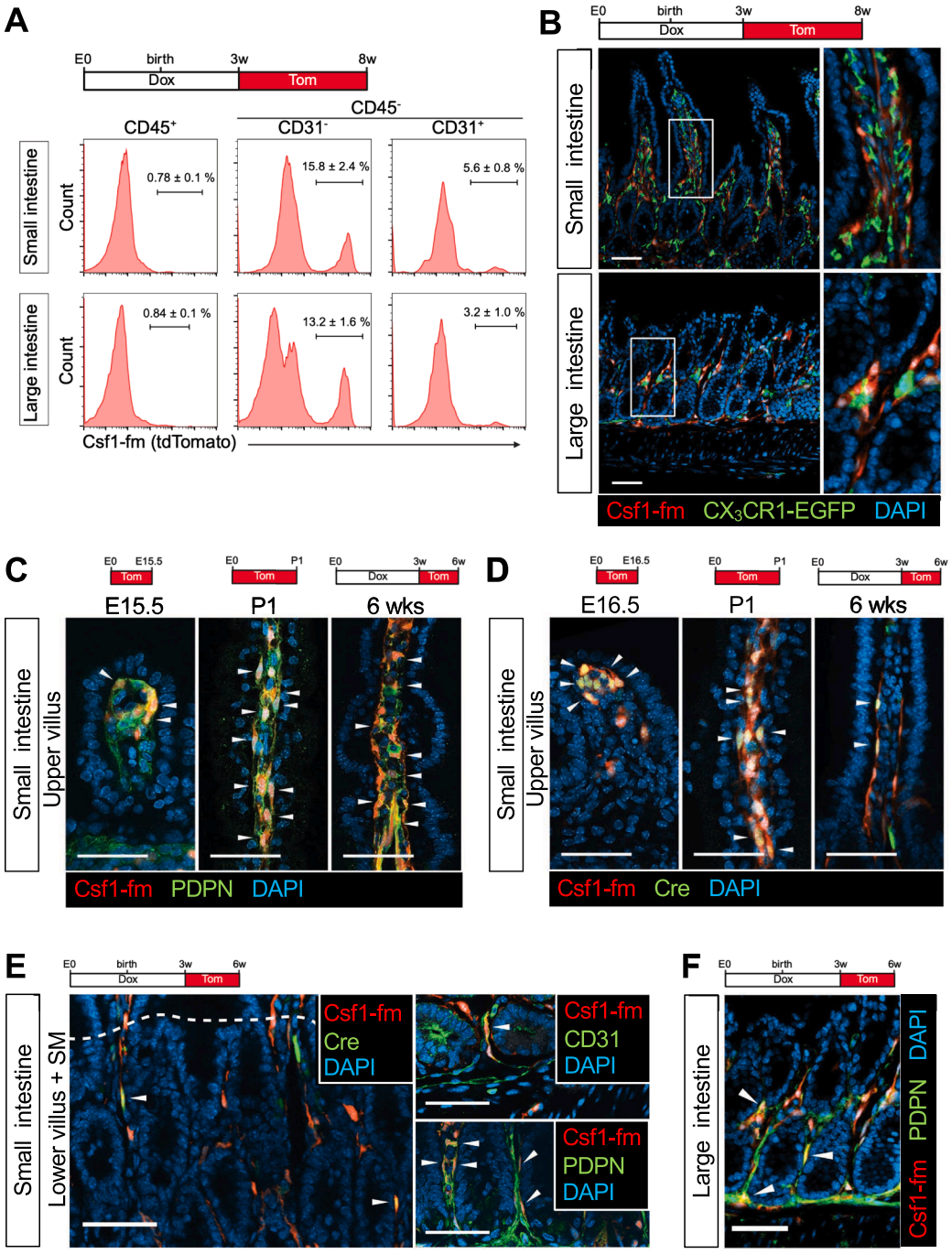

Fig. 2. Histological analysis of *Csf1*-expressing cells in the intestine. (A) Flow cytometry analysis of small and large intestines from 8-week-old *Csf1*$^{tTA/+}$; *LC1*; *Rosa26*$^{LSL\text{-}tdTomato}$ mice treated with 50 μg/mL doxycycline in drinking water from embryonic day 0 (E0) until 3 weeks after birth, followed by normal water. Representative histograms show tdTomato$^+$ cells within CD45.2$^+$ (left), CD45.2$^-$ CD31$^-$ (middle), and CD45.2$^-$ CD31$^+$ (right) populations. Mean ± SEM values (%) are indicated. Small intestine: n = 4; large intestine: n = 3. Numbers indicate percentages of gated populations. (B) Representative confocal microscopy images of intestinal sections from *Csf1*$^{tTA/+}$; *LC1*; *Rosa26*$^{LSL\text{-}tdTomato}$; *Cx3cr1*$^{gfp/+}$ mice. Small (upper panels) and large (lower panels) intestines of 6-week-old mice in which Dox was withdrawn at 3 weeks of age. Right panels show magnified views of boxed regions in the left panels. CSF1-fate mapped cells, macrophages, and nuclei are visualized as Csf1-fm (red), CX_3CR1-EGFP (green), and DAPI, respectively. Scale bars, 50 μm. (C-F) Representative confocal microscopy images of intestinal sections from *Csf1*$^{tTA/+}$; *LC1*; *Rosa26*$^{LSL\text{-}tdTomato}$ mice. (C) Immunofluorescence of jejunal upper villus regions from perinatal (E15.5 and P1) mice maintained under Dox-free condition, and 6-week-old mice after 3 weeks of age. CSF1-fate mapped cells, PDPN$^+$ fibroblasts, and nuclei are visualized as Csf1-fm (red), PDPN (green), and DAPI. Arrowheads indicate PDPN$^+$ tdTomato$^+$ cells. Scale bars, 50 μm. (D) Immunofluorescence of jejunal upper villus region from perinatal (E16.5 and P1) mice under Dox-free conditions, and 6-week-old mice after Dox withdrawal at 3 weeks of age. *Csf1*-fate-mapped cells, Cre-expressing cells, and nuclei are visualized as Csf1-fm (red), Cre (green), and DAPI. Arrowheads indicate Cre$^+$ tdTomato$^+$ cells. Scale bars, 50 μm. (E) Immunofluorescence of jejunal lower villus + SM region from 6-week-old mice following Dox withdrawal at 3 weeks of age. Left: Csf1-fm (red), Cre (green), and DAPI. Arrowheads indicate Cre$^+$ tdTomato$^+$ cells in the villus. Right upper: Csf1-fm (red), CD31 (green), and DAPI. Arrowheads indicate CD31$^+$ tdTomato$^+$ cells. Right lower: Csf1-fm (red), PDPN (green), and DAPI. Arrowheads indicate PNPD$^+$ tdTomato$^+$ fibroblasts. Scale bars, 50 μm. (F) Immunofluorescence of distal large intestinal sections 6-week-old mice following Dox withdrawal at 3 weeks of age. CSF1-fate-mapped cells, PDPN$^+$ fibroblasts, and nuclei are visualized as Csf1-fm (red), PDPN (green), and DAPI. Arrowheads indicate PDPN$^+$ tdTomato$^+$ cells. Scale bars, 50 μm.

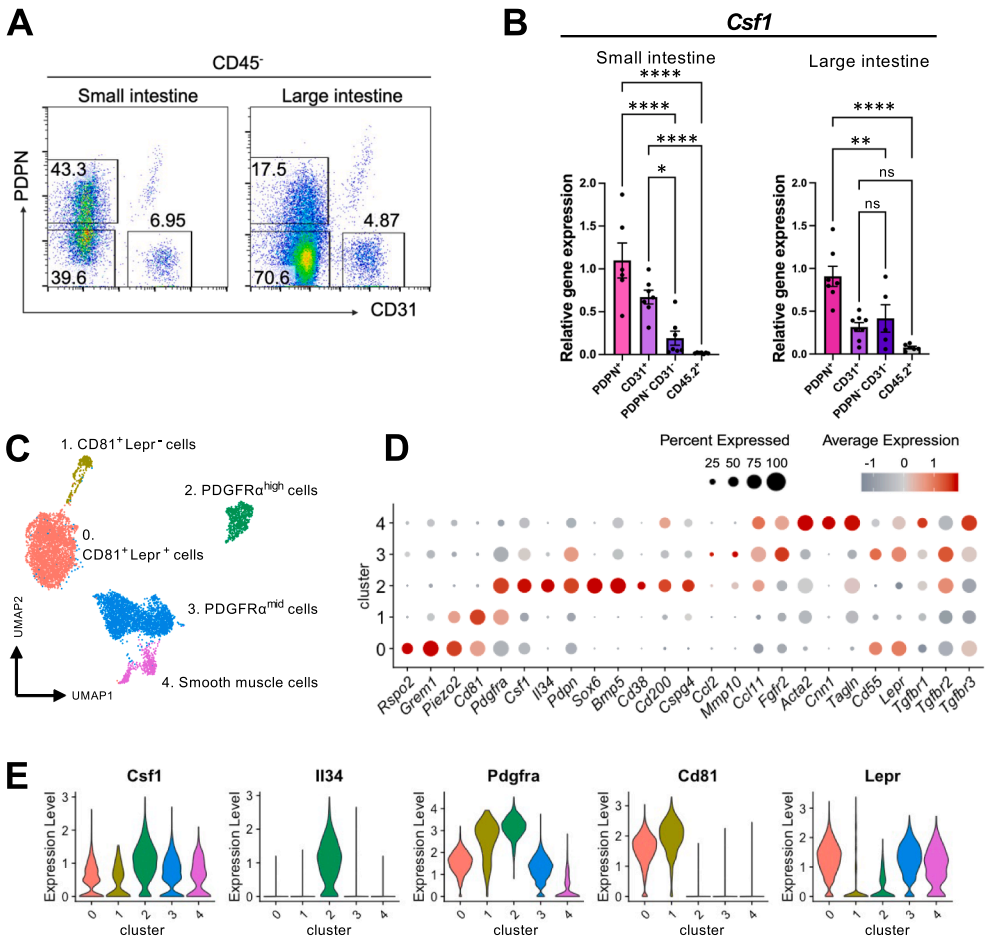

Fig. 3. Transcriptomic analysis of *Csf1*-expressing cells in the intestine. (A) Flow cytometry analysis of the small (left) or large intestine (right) from 6-week-old wild type (WT) mouse. Shown are representative expression patterns of PDPN and CD31 among CD45.2$^-$. Numbers indicate the percentages of gated populations. (B) *Csf1* expression levels in intestinal cells from 6-week-old WT mice analyzed by quantitative PCR. PDPN$^+$ (n = 6 for SI, n = 7 for LI), CD31$^+$ (n = 7 for SI, n = 8 for SI), PDPN$^-$ CD31$^-$ (n = 7 for SI, n = 5 for LI), and CD45$^+$ cells (n = 7 for SI, n = 6 for LI) represent PDPN$^+$ fibroblasts, CD31$^+$ endothelial cells, PDPN$^-$ CD31$^-$ mesenchymal cells, and CD45$^+$ hematopoietic cells, respectively. The experiment was performed twice for the small intestine (SI) and three times for the large intestine (LI). Data are shown as mean ± SEM. Statistical analysis was performed using one-way ANOVA followed by Sidak's multiple comparison test. *$p < 0.05$, **$p < 0.01$, ****$p < 0.001$; ns, indicates not significant. (C) Uniform Manifold Approximation and Projection (UMAP) plot of PDPN$^+$ fibroblast isolated from the small intestine of 4-week-old wild type mice, revealing five distinct clusters. Each dot represents a single cell. (D) Dot plot showing the expression of selected marker genes across the clusters identified in (C). (E) Violin plots displaying the expression levels of *Csf1*, *Il34*, *Pdgfra*, *Cd81*, and *Lepr* in the clusters identified in (C).

with previously reported intestinal mesenchymal populations[41,44,45] (Fig. 3C–E, Supplementary Fig. 4A, B). Cluster 0 was identified as CD81$^+$ LepR$^+$ fibroblasts, corresponding to previously reported populations such as CD81$^+$ fibroblasts[44], FB4[45], or trophocytes[40,41], based on their high expression of *Lepr*, *Cd81*, *Grem1*, and *Piezo2*. Cluster 1, termed CD81$^+$ LepR$^-$ fibroblasts, also exhibited high expression of *Cd81* and *Piezo2* but showed lower levels of *Lepr* and *Cd55* compared to Cluster 0. Cluster 2 was classified as PDGFRα^{high} fibroblasts[44], also known as FB5[45] or telocytes/subepithelial myofibroblasts[40,46]. These cells were characterized by high expression of *Sox6*, *Bmp5*, and *Pdgfra*. Cluster 3, defined as PDGFRα^{mid} fibroblasts, expressed *Ccl11*, *Fgfr2*, *Lepr*, and intermediate levels of *Pdgfra*. This cluster largely overlapped with the Lo-2 subset[41], encompassing *Igfbp5*$^+$ and *Fgfr2*$^+$ fibroblasts[44], as well as FB2 and FB3[45]. Cluster 4 was annotated as smooth muscle cells, based on their expression of myosin-related genes, such as *Myh11* and *Myl9* (Supplementary Fig. 4A).

We also performed scRNA-seq analysis on PDPN$^+$ fibroblasts from the large intestine. Based on previous reports, these cells were categorized into three clusters: Cluster 0, identified as CD81$^-$ fibroblasts (overlapping with CD90$^+$ FB and Fgfr2$^+$ FB[44], as well as CD81$^-$ stroma[42]), Cluster 1, CD81$^+$ fibroblasts (equivalent to CD81$^+$ FB[39] and trophocytes[47]), and Cluster 2, PDGFRα^{high} fibroblasts (corresponding to PDGFRα^{high} FB[44] and SEMF[47]) (Supplementary Fig. 5).

In the small and large intestines, *Csf1* was highly expressed in all clusters, including smooth muscle cells (Fig. 3E, Supplementary Fig. 5D). Notably, in the small intestine, PDGFRα^{high} cells exhibited the highest *Csf1* expression (Fig. 3E). Consistent with these findings, subepithelial PDPN$^+$ fibroblasts– presumably PDGFRα^{high} cells–in *Csf1*$^{tTA/+}$; *LC1*; *Rosa26*$^{LSL\text{-}tdTomato}$ mice expressed Cre, indicating continuous *Csf1* promoter activity (Fig. 2D).

Taken together, these findings indicate that PDPN$^+$ fibroblasts are the primary producers of CSF1 in the lamina propria of the small and large intestines. Among PDPN$^+$ fibroblast subpopulations, PDGFRα^{high} cells prominently express both CSF1 and IL-34.

Fibroblasts compose the microenvironment required for gut mucosal macrophages

Ubiquitous *Csf1* expression across all subsets of PDPN$^+$ fibroblasts (Fig. 3E, Supplementary Fig. 5D) strongly suggests that gut macrophages are primarily maintained by fibroblast-derived CSF1. However, whether distinct macrophage subsets establish their own niche composed of specific local CSF1-producing fibroblast subsets remains unknown. To investigate this, we generated a series of cell lineage-specific *Csf1*-

deficient mouse lines using several Cre drivers.

To investigate the role of mesenchymal cell-derived CSF1, we crossed *Twist2*$^{Cre/+}$ mice[48] with *Csf1*$^{fl/fl}$ mice[49]. Fate-mapping analysis using the *Rosa26*$^{LSL\text{-}tdTomato}$ reporter line confirmed that the *Twist2*$^{Cre/+}$ line targets PDPN^{+} fibroblasts and CD31^{+} endothelial cells (Supplementary Fig. 6A, B). In *Twist2*$^{Cre/+}$; *Csf1*$^{fl/fl}$ mice, macrophage density in the small intestine was reduced by approximately 30 % in the upper villus region and 70 % in the lower villus + SM region (Fig. 4A, B). This reduction was even more pronounced in *Twist2*$^{Cre/+}$; *Csf1*$^{fl/fl}$; *Il34*$^{-/-}$ mice, particularly within the upper villus, indicating that IL-34 partially compensates for CSF1 deficiency in maintaining upper villus macrophages (Fig. 4A–C). Flow cytometry analysis further supported the histological findings, showing a significant reduction in the overall macrophage frequency in the small intestine of *Twist2*$^{Cre/+}$; *Csf1*$^{fl/fl}$ mice, with a further decrease observed in *Twist2*$^{Cre/+}$; *Csf1*$^{fl/fl}$; *Il34*$^{-/-}$ mice (Fig. 4D). These results demonstrate that fibroblast-derived CSF1 is

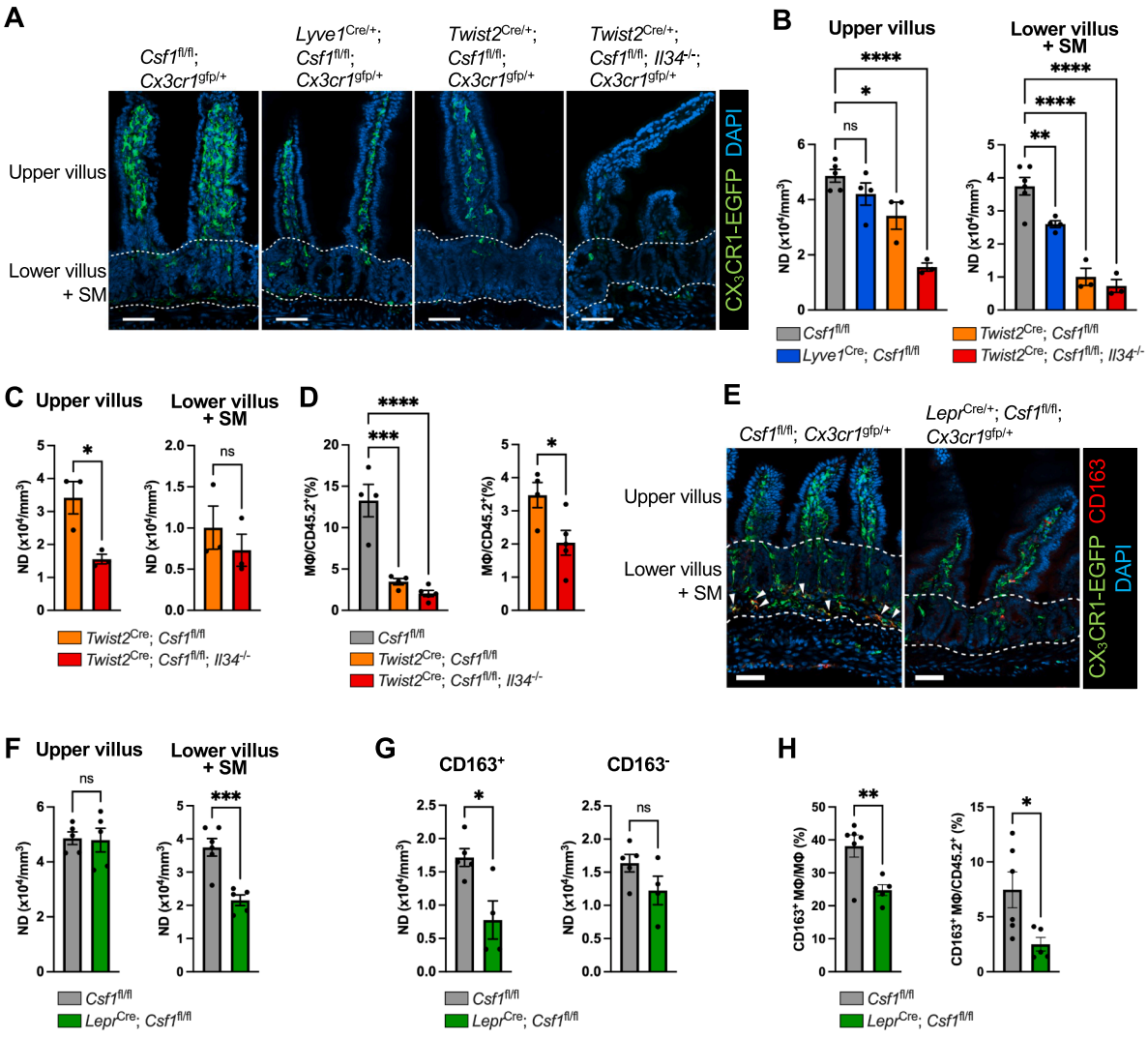

Fig. 4. Fibroblasts form the microenvironment required for gut mucosal macrophages. (A) Representative confocal images of jejunum sections from 4-week-old *Csf1*$^{fl/fl}$; *Cx3cr1*$^{gfp/+}$, *Lyve1*$^{Cre/+}$; *Csf1*$^{fl/fl}$; *Cx3cr1*$^{gfp/+}$, *Twist2*$^{Cre/+}$; *Csf1*$^{fl/fl}$; *Cx3cr1*$^{gfp/+}$, and *Twist2*$^{Cre/+}$; *Csf1*$^{fl/fl}$; *Il34*$^{-/-}$; *Cx3cr1*$^{gfp/+}$ mice. Macrophages and nuclei are visualized as CX_3CR1-EGFP and DAPI, respectively. Dashed lines delineate the boundaries between the upper villus, lower villus + SM, and muscularis externa. Scale bars, 50 μm. (B, C) Quantification of macrophages in the upper villus (left) and lower villus + SM (right) regions of jejunal sections from 4-week-old *Csf1*$^{fl/fl}$; *Cx3cr1*$^{gfp/+}$ (n = 6), *Lyve1*$^{Cre/+}$; *Csf1*$^{fl/fl}$; *Cx3cr1*$^{gfp/+}$ (n = 4), *Twist2*$^{Cre/+}$; *Csf1*$^{fl/fl}$; *Cx3cr1*$^{gfp/+}$ (n = 3), and *Twist2*$^{Cre/+}$; *Csf1*$^{fl/fl}$; *Il34*$^{-/-}$; *Cx3cr1*$^{gfp/+}$mice (n = 3) (B). Panel (C) shows re-analysis of the data for *Twist2*$^{Cre/+}$; *Csf1*$^{fl/fl}$; *Cx3cr1*$^{gfp/+}$ and *Twist2*$^{Cre/+}$; *Csf1*$^{fl/fl}$; *Il34*$^{-/-}$; *Cx3cr1*$^{gfp/+}$mice. Numerical densities were calculated from images shown in. (A). Experiments were performed twice for *Twist2*$^{Cre/+}$; *Csf1*$^{fl/fl}$; *Cx3cr1*$^{gfp/+}$ mice, three times for *Lyve1*$^{Cre/+}$; *Csf1*$^{fl/fl}$; *Cx3cr1*$^{gfp/+}$ mice and twice for *Twist2*$^{Cre/+}$; *Csf1*$^{fl/fl}$; *Il34*$^{-/-}$; *Cx3cr1*$^{gfp/+}$ mice. (D) Flow cytometry analysis of small intestinal macrophages from 4-week-old *Csf1*$^{fl/fl}$ (n = 4), *Twist2*$^{Cre/+}$; *Csf1*$^{fl/fl}$ (n = 4), and *Twist2*$^{Cre/+}$; *Csf1*$^{fl/fl}$; *Il34*$^{-/-}$ (n = 5) mice (left). The same data for *Twist2*$^{Cre/+}$; *Csf1*$^{fl/fl}$ and *Twist2*$^{Cre/+}$; *Csf1*$^{fl/fl}$; *Il34*$^{-/-}$ mice were re-analyzed (right). Frequencies of CD11b^{+} CD64^{+} Ly6C^{low} MHCII^{high} cells among CD45.2^{+} cells are shown. (E) Representative confocal images of jejunal sections from 4-week-old *Csf1*$^{fl/fl}$; *Cx3cr1*$^{gfp/+}$ and *Lepr*$^{Cre/+}$; *Csf1*$^{fl/fl}$; *Cx3cr1*$^{gfp/+}$ mice. Macrophages (CX_3CR1-EGFP), CD163, and nuclei (DAPI) are shown. Dashed lines indicate boundaries between the upper villus, lower villus + SM, and muscularis externa. Scale bars, 50 μm. (F) Quantification of macrophages in the upper villus (left) and lower villus + SM (right) regions from 4-week-old *Csf1*$^{fl/fl}$; *Cx3cr1*$^{gfp/+}$ (n = 5) and *Lepr*$^{Cre/+}$; *Csf1*$^{fl/fl}$; *Cx3cr1*$^{gfp/+}$ (n = 5) mice. Numerical densities were calculated from images shown in (E). (G) Quantification of CD163^{+} (left) and CD163^{-} (right) macrophages in the lower villus + SM region from 4-week-old *Csf1*$^{fl/fl}$; *Cx3cr1*$^{gfp/+}$(n = 5) and *Lepr*$^{Cre/+}$; *Csf1*$^{fl/fl}$; *Cx3cr1*$^{gfp/+}$ (n = 4) mice. Numerical densities were calculated from images in (E). Experiments were performed four times. (H) Flow cytometry analysis of small intestinal macrophages from 4-week-old *Csf1*$^{fl/fl}$; *Cx3cr1*$^{gfp/+}$ (n = 6) and *Lepr*$^{Cre/+}$; *Csf1*$^{fl/fl}$; *Cx3cr1*$^{gfp/+}$ (n = 5) mice. Frequencies of CD163^{+} macrophages among total CD45^{+} cells (left) and among total macrophages (right) are shown. Data represent pooled results from at least two independent experiments and are presented as mean ± SEM. Statistical analyses were conducted using one-way ANOVA with Dunnett's multiple comparison test (B), and unpaired *t*-test (C, D, F-H). Statistical significance is indicated as $*p < 0.05$, $**p < 0.01$, $***p < 0.001$, $****p < 0.0001$; ns, not significant.

essential for maintaining the entire mucosal macrophage compartment, while IL-34 provides additional support specifically for upper villus macrophages. Similar trends were observed in the large intestine (Supplementary Fig. 7).

Given that *Csf1* mRNA was detectable in CD31$^+$ endothelial cells (Fig. 3B), endothelial cell-derived CSF1 is likely to be functionally relevant. To assess its contribution, we utilized the *Lyve1*$^{Cre/+}$ line[50]. In *Lyve1*$^{Cre/+}$; *Csf1*$^{fl/fl}$ mice, macrophage density in the lower villus + SM region was significantly reduced, while upper villus macrophages remained unaffected (Fig. 4A, B). Previous studies have reported that both fetal and adult hematopoietic stem cells (HSCs) exhibit 35–40 % *Lyve1*^{Cre} activity[51], resulting in 50–70 % of tdTomato labeling in blood leukocytes of *Lyve1*$^{Cre/+}$; *Rosa26*$^{LSL\text{-}tdTomato}$ reporter mice[52] (Supplementary Fig. 6C). However, CD45$^+$ hematopoietic cells express markedly lower levels of *Csf1* mRNA compared to endothelial cells (Fig. 3A, B). Thus, the reduced macrophage density in the lower villus + SM region in *Lyve1*$^{Cre/+}$; *Csf1*$^{fl/fl}$ mice is most likely due to the loss of CSF1 from endothelial cells rather than from hematopoietic sources. Collectively, these findings suggest that upper villus macrophages are maintained cooperatively by fibroblast-derived CSF1 and IL-34, while macrophages in the lower villus + SM region primarily depend on fibroblast-derived CSF1 and, to a lesser extent, on endothelial cell-derived CSF1.

CD163$^+$ macrophages are enriched in tumorigenic and inflammatory microenvironments[53]. In gut macrophages, CD163 expression is induced by anti-inflammatory cytokine IL-10[54]. Given their immunomodulatory role, we sought to identify the niches of CD163$^+$ macrophages in the intestine. Our scRNA-seq analysis of gut PDPN$^+$ cells revealed high *Lepr* expression within *Cd81*$^+$ fibroblasts, *Fgfr2*$^+$ PDGFRα^{mid} fibroblasts and smooth muscle cells (Fig. 3D, E). Among these, using the *Lepr*$^{Cre/+}$ mouse line[55], we identified LepR$^+$ fibroblasts predominantly localized in the lower villus + SM region (Supplementary Fig. 6D), where CD163$^+$ macrophages are exclusively found[56] (Fig. 4E, Supplementary Fig. 9). Flowcytometry analysis confirmed that tdTomato$^+$ cells were selectively observed within the CD81$^+$ population among PDPN$^+$ cells in *Lepr*$^{Cre/+}$; *Rosa26*$^{LSL\text{-}tdTomato}$ mice (Supplementary Fig. 6E), suggesting that *Lepr*$^{Cre/+}$ is a suitable Cre driver for targeting CD81$^+$ LepR$^+$ fibroblasts, but not for other LepR$^+$ cells such as smooth muscle cells. To assess the functional relevance of CD81$^+$ LepR$^+$ fibroblast-derived CSF1 in maintaining CD163$^+$ macrophages, we generated *Lepr*$^{Cre/+}$; *Csf1*$^{fl/fl}$ mice. In these mice, lower villus + SM macrophage density was significantly reduced, with a marked depletion of CD163$^+$ macrophages within the lower villus + SM region (Fig. 4E–H). Notably, CD163$^+$ macrophage numbers remained unchanged in *Lyve1*$^{Cre/+}$; *Csf1*$^{fl/fl}$ mice (Supplementary Fig. 10), indicating that CD81$^+$ LepR$^+$ fibroblasts, rather than endothelial cells, are the primary source of CSF1 for CD163$^+$ macrophages located in the lower villus + SM region.

Taken together, these findings establish that fibroblast-derived CSF1 plays a predominant role in gut macrophage maintenance. In particular, the number of CD163$^+$ macrophages is tightly regulated by CSF1 derived from lower villus-specific CD81$^+$ LepR$^+$ fibroblasts, highlighting fibroblasts as a key component of the gut mucosal macrophage niche.

CSF1 is essential for the proliferation and maturation of perinatal intestinal macrophages

Intestinal macrophages originate from two distinct sources: fetus-derived macrophages and adult bone marrow (BM)-derived macrophages[57]. Following weaning, fetus-derived macrophages are largely replaced by BM-derived macrophages, although a subset persists through self-renewal[5,6,19].

To evaluate the dependence of fetus-derived macrophages on CSF1, we analyzed the intestines of P0 *Twist2*$^{Cre/+}$; *Csf1*$^{fl/fl}$ mice. In these mice, the frequency of Ki67$^+$ proliferating intestinal macrophages was significantly reduced compared to controls (Fig. 5A–C). Conversely, the frequency of Ly6C^{high} monocytes in P0 intestine was increased (Fig. 5D, Supplementary Fig. 8A), suggesting that CSF1 is crucial for the proliferation and differentiation of fetus-derived monocytes into intestinal macrophages immediately after birth.

Local CSF1 in the gut supports the colonization of BM-derived macrophages

We next investigated the role of CSF1 in the colonization of BM-derived macrophages after weaning[6,58]. Although the absolute number of Ly6C^{high} monocytes in the BM of *Twist2*$^{Cre/+}$; *Csf1*$^{fl/fl}$ mice was slightly lower than that of controls, their frequency in the BM and concentration in the peripheral blood remained comparable (Supplementary Fig. 8B, C). Notably, despite similar numbers of circulating monocytes, the direct precursors of intestinal macrophages, the frequencies of Ly6C^{high} MHCII^{low} monocytes and macrophages in both the small and large intestines were markedly reduced in *Twist2*$^{Cre/+}$; *Csf1*$^{fl/fl}$ mice at eight weeks of age (Fig. 5E, F). Nevertheless, serum CSF1 levels were significantly lower than in *Csf1*$^{fl/fl}$ mice (Supplementary Fig. 8D). These findings suggest that systemic and intestinal fibroblast-derived CSF1 is dispensable for maintaining blood monocyte levels. Instead, we hypothesized that fibroblast-derived CSF1 plays a critical role in the recruitment and differentiation of monocytes into mature intestinal macrophages.

To evaluate contribution of CSF1 to the colonization of BM-derived monocytes, we employed a parabiosis model[59] to establish shared blood circulation between CD45.1/CD45.2; *Cx3cr1*$^{gfp/+}$ donor mice and CD45.2/CD45.2; *Twist2*$^{Cre/+}$; *Csf1*$^{fl/fl}$ or CD45.2/CD45.2; *Csf1*$^{fl/fl}$ recipient mice (Fig. 5G). Eight weeks after surgery, peripheral blood chimerism was comparable between *Csf1*$^{fl/fl}$ and *Twist2*$^{Cre/+}$; *Csf1*$^{fl/fl}$ mice, ensuring equal systemic monocyte availability (Fig. 5H). However, in *Twist2*$^{Cre/+}$; *Csf1*$^{fl/fl}$ recipients, donor-derived (EGFP$^+$) macrophages were significantly fewer in the small intestine compared to *Csf1*$^{fl/fl}$ controls, despite equivalent circulating monocytes (Fig. 5I). The number of donor-derived macrophages colonizing the small and large intestines was also significantly lower in *Twist2*$^{Cre/+}$; *Csf1*$^{fl/fl}$ recipients (Fig. 5J, K). These findings suggest that gut-derived CSF1 is necessary for the efficient recruitment and differentiation of BM-derived monocytes into mature macrophages in the intestine.

Recently, Tim4 has been proposed as a marker of long-lived macrophages[19,60,61], most of which are fetus-derived in the intestine. In this study, we confirmed that the majority of CD163$^+$ macrophages express Tim4[56], and that their numbers are significantly reduced in *Twist2*$^{Cre/+}$; *Csf1*$^{fl/fl}$ mice (Supplementary Fig. 11). These findings led us to investigate whether CSF1 influences the differentiation of monocyte-derived macrophages into CD163$^+$ macrophages in the gut. In *Twist2*$^{Cre/+}$; *Csf1*$^{fl/fl}$ recipients, the percentage of CD163$^+$ macrophages among donor-derived macrophages was significantly lower compared to control parabionts (Fig. 5L, M). Given their Tim4 expression, CD163$^+$ macrophages in the small intestine are likely long-lived, presumably fetus-derived, and dependent on CD81$^+$ LepR$^+$ fibroblast-derived CSF1 for their intestinal colonization.

*Fibroblast-derived CSF1 contributes to resistance against **S. Typhimurium** infection*

To assess the biological significance of CSF1-dependent macrophages, we examined host resistance to *S.* Typhimurium, a well-established cause of enteritis. We orally infected lineage-specific CSF1-deficient mice with *S.* Typhimurium one day after streptomycin pretreatment[62] to disrupt the intestinal microbiota (Fig. 6A). By day 6 post-infection, 90 % of *Twist2*$^{Cre/+}$; *Csf1*$^{fl/fl}$ mice had succumbed, whereas *Lyve1*$^{Cre/+}$; *Csf1*$^{fl/fl}$ and *Lepr*$^{Cre/+}$; *Csf1*$^{fl/fl}$ mice exhibited survival rates comparable to those of control *Csf1*$^{fl/fl}$ mice (Fig. 6B). These findings suggest that CSF1 derived from fibroblasts, excluding CD81$^+$ LepR$^+$ submucosa-specific fibroblasts, plays a critical role in host defense

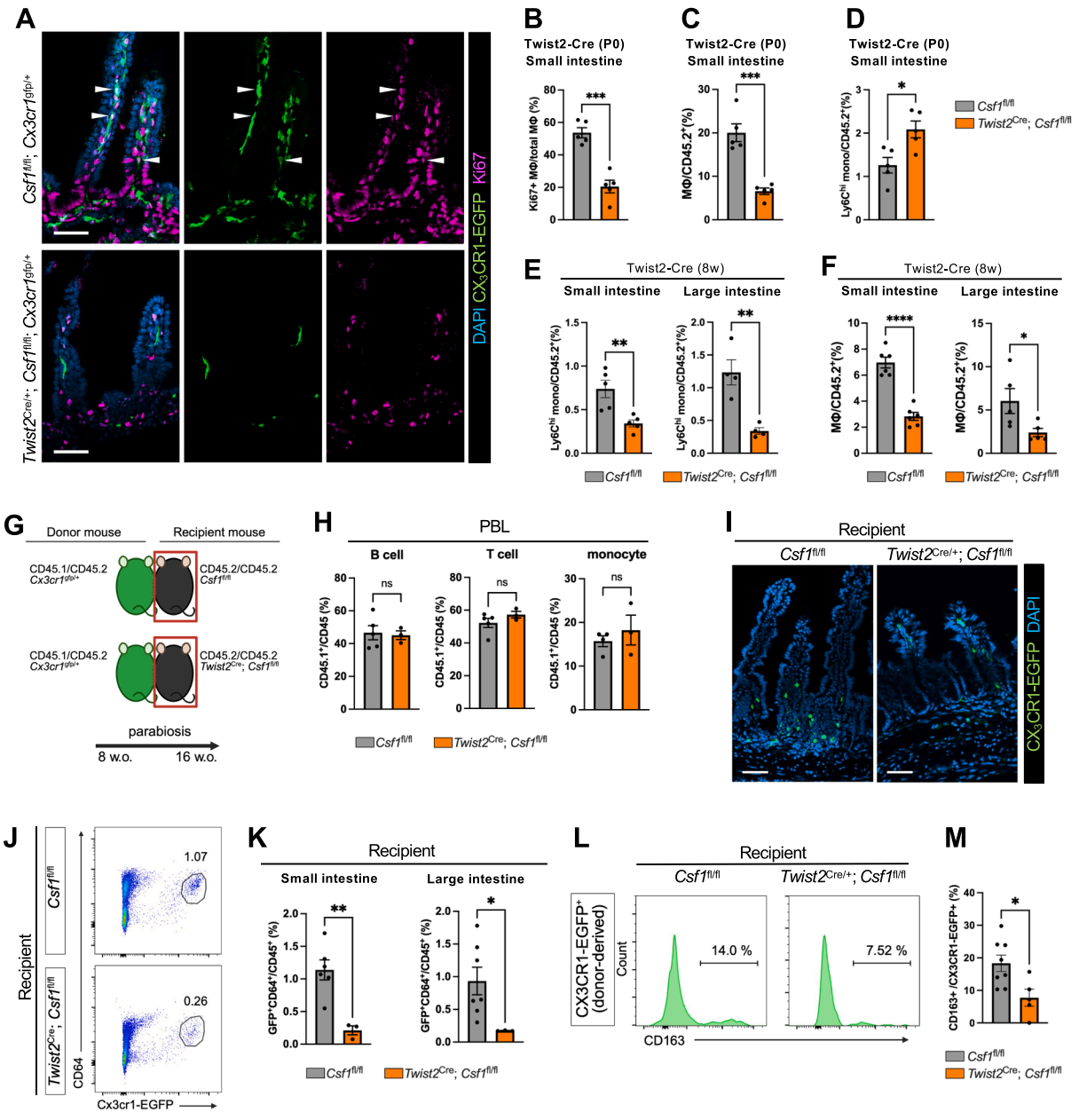

Fig. 5. Intestinal fibroblast-derived CSF1 supports colonization of mucosal macrophages. (A) Representative immunofluorescence images of the jejunal sections from P0 *Csf1*$^{fl/fl}$; *Cx3cr1*$^{gfp/+}$ (upper panels) and *Twist2*$^{Cre/+}$; *Csf1*$^{fl/fl}$; *Cx3cr1*$^{gfp/+}$ (lower panels) mice. Macrophages and proliferating cells are visualized by CX_3CR1-EGFP and Ki67, respectively. Merged (left), CX_3CR1-EGFP (middle), and Ki67 (right) images were shown. Nuclei are stained with DAPI. Arrowheads indicate Ki67$^+$ CX_3CR1-EGFP$^+$ cells. Scale bars, 50 μm. (B) Frequencies of Ki67$^+$ cells among CX_3CR1-EGFP$^+$ cells in the small intestine of P0 *Csf1*$^{fl/fl}$; *Cx3cr1*$^{gfp/+}$ and *Twist2*$^{Cre/+}$; *Csf1*$^{fl/fl}$; *Cx3cr1*$^{gfp/+}$ mice (n = 5 per group), based on data from (A). The experiment was performed twice. (C, D) Flow cytometry analysis of small intestinal macrophages in P0 *Csf1*$^{fl/fl}$; *Cx3cr1*$^{gfp/+}$ and *Twist2*$^{Cre/+}$; *Csf1*$^{fl/fl}$; *Cx3cr1*$^{gfp/+}$mice (n = 5 per group). Frequencies of CD11b$^+$ CD64$^+$ Ly6C^{low} MHCII^{high} macrophages (C) and CX_3CR1-EGFP^{mid} Ly6C^{high} monocytes (D) among CD45.2$^+$ cells are shown. The experiment was performed twice. (E, F) Frequencies of CD11b$^+$ CD64$^+$ Ly6C^{high} MHCII^{low} immature monocytes (E) and CD11b$^+$ CD64$^+$ Ly6C^{low} MHCII^{high} macrophages (F) among CD45.2$^+$ cells in the small and large intestine of 8-week-old *Csf1*$^{fl/fl}$ and *Twist2*$^{Cre/+}$; *Csf1*$^{fl/fl}$ mice. n = 5 per group for (E), n-6 (small intestine) and n = 5 (large intestine) for (F). The experiment was performed three times. (G) Schematic of the parabiosis experiment. Eight-week-old CD45.1$^+$; *Cx3cr1*$^{gfp/+}$ mice (green) were surgically joined with either *Csf1*$^{fl/fl}$ or *Twist2*$^{Cre/+}$; *Csf1*$^{fl/fl}$ mice (black). Recipient mice (red outline) were sacrificed 8 weeks after surgery. (H) Frequencies of CD45.1$^+$ CD3ε$^+$ T cells, CD45.1$^+$ B220$^+$ B cells and CD45.1$^+$ CD11b$^+$ Ly6C^{high} monocytes among total CD45$^+$ hematopoietic cells in the peripheral blood of CD45.2/CD45.2; *Csf1*$^{fl/fl}$ (n = 5) and CD45.2/CD45.2; *Twist2*$^{Cre/+}$; *Csf1*$^{fl/fl}$ (n = 3) parabionts. The experiment was performed three times. (I) Representative confocal images of the jejunal sections from *Csf1*$^{fl/fl}$ or *Twist2*$^{Cre/+}$; *Csf1*$^{fl/fl}$ parabiosis recipients, showing donor-derived CX_3CR1-EGFP$^+$ macrophages (green) and DAPI-stained nuclei (blue). Scale bar, 50 μm. The experiment was performed twice. (J) Flow cytometry analysis of small intestinal lamina propria cells obtained from parabiosis recipients. Expression of CD64 and CX_3CR1-EGFP is shown. Numbers indicate percentages of gated populations. The experiment was performed twice. (K) Frequencies of CX_3CR1-EGFP$^+$CD64$^+$ cells in the small (left) and large (right) intestines of parabiosis recipient *Csf1*$^{fl/fl}$ (SI: n = 6, LI: n = 7) and *Twist2*$^{Cre/+}$; *Csf1*$^{fl/fl}$ (SI: n = 3, LI: n = 3) mice. Data were obtained from flow cytometry as shown in (J). The experiment was performed three times. (L, M) Flow cytometry analysis of small intestinal lamina propria macrophages from *Csf1*$^{fl/fl}$(n = 8) or *Twist2*$^{Cre/+}$; *Csf1*$^{fl/fl}$ (n = 5) parabiosis recipients. (L) CD163 expression in donor-derived CX3CR1-EGFP$^+$ macrophages; numbers indicate percentages of gated populations. (M) Frequencies of CD163$^+$ cells among donor-derived macrophages. The experiments were performed four times. Data represent pooled results from at least two independent experiments and are presented as mean ± SEM. Statistical analyses were conducted using unpaired *t*-tests (B-D, E, F, H, K-SI, M) and the Mann-Whitney test (K-LI). Statistical significance is indicated as *p < 0.05, **p < 0.01, ***p < 0.001, ****p < 0.0001; ns, not significant.

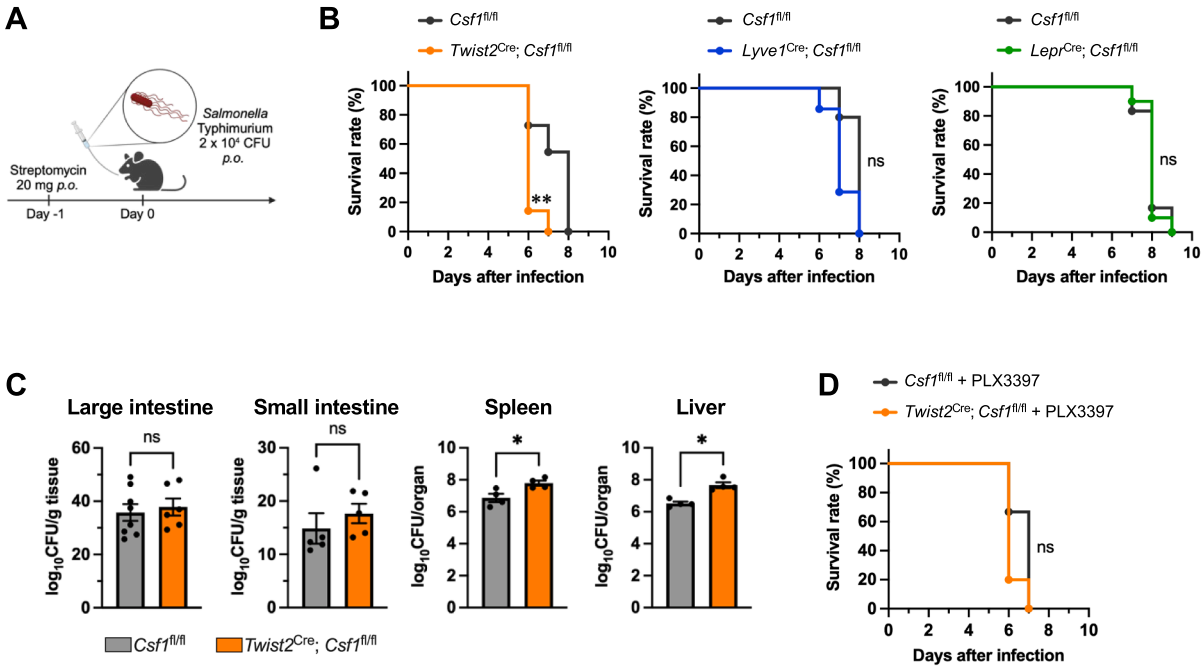

Fig. 6. Fibroblast-derived CSF1 contributes to the resistance against *Salmonella* Typhimurium infection. (A) Experimental design for *S.* Typhimurium infection experiments. Ten-week-old female C57BL/6J mice were administered streptomycin (20 mg) via oral gavage 24 h before oral infection with *S.* Typhimurium (SL1344 strain 2x10^4 CFU). For experiments in (D), mice were fed a PLX3397-containing diet for 2 weeks prior to infection. (B) Kaplan–Meier survival curves of *S.* Typhimurium-infected mice: *Csf1*$^{fl/fl}$ (n = 11) and *Twist2*$^{Cre/+}$; *Csf1*$^{fl/fl}$ (n = 7) (left), *Csf1*$^{fl/fl}$ (n = 5) and *Lyve1*$^{Cre/+}$; *Csf1*$^{fl/fl}$ (n = 10) (center), *Csf1*$^{fl/fl}$ (n = 6), and *Lepr*$^{Cre/+}$; *Csf1*$^{fl/fl}$ (n = 10) (right). Each dataset represents pooled results from two independent experiments. Statistical analysis was performed suing log-rank (Mantel-Cox) test. **p < 0.01; ns, not significant. (C) Bacteria loads of *S.* Typhimurium in the indicated organs from *Csf1*$^{fl/fl}$ (control) and *Twist2*$^{Cre/+}$; *Csf1*$^{fl/fl}$ (cKO) mice four days post-infection. CFU counts in the large intestine (control: n = 8, cKO: n = 6), small intestine (n = 5 each), spleen (n = 4 each), and liver (n = 4 each) were normalized to tissue weight. Data represent pooled results from four independent experiments and are shown as mean ± SEM. Statistical analysis was performed using an unpaired *t*-test. *p < 0.05; ns, not significant. (D) Kaplan–Meier survival curve of *Csf1*$^{fl/fl}$ (n = 6) and *Twist2*$^{Cre/+}$; *Csf1*$^{fl/fl}$ (n = 5) mice fed a PLX3397-containing diet for 2 weeks prior to *S.* Typhimurium infection. Data represent pooled results from two independent experiments. Statistical analysis was conducted using the log-rank (Mantel-Cox) test. ns, not significant.

against *S.* Typhimurium.

Despite comparable bacterial loads in the intestines of *Twist2*$^{Cre/+}$; *Csf1*$^{fl/fl}$ and control mice, systemic dissemination of *S.* Typhimurium to the spleen and liver was significantly increased in the *Twist2*$^{Cre/+}$; *Csf1*$^{fl/fl}$ group (Fig. 6C). This suggests that CSF1 produced by fibroblast restricts bacterial spread beyond the intestine.

To determine whether macrophage reduction was the primary driver of early mortality, we pretreated *Twist2*$^{Cre/+}$; *Csf1*$^{fl/fl}$ mice with PLX3397[33], a potent CSF1R inhibitor (Fig. 1A–C), before infection. Macrophage depletion resulted in infection severity comparable to that observed in control *Csf1*$^{fl/fl}$ mice (Fig. 6D). These results confirm that fibroblast-derived CSF1 supports gut macrophages, which in turn limit systemic *S.* Typhimurium dissemination. Loss of fibroblast-derived CSF1 compromises host defense, leading to increased bacterial spread and mortality.

Discussion

Macrophages are widely distributed across tissues in diverse organisms, from metazoans to vertebrates, where they play critical roles in tissue homeostasis[3]. While it is well established that resident macrophages form distinct populations depending on their origin and microenvironment[63], how intestinal macrophages are maintained by local niche factors remains incompletely understood.

In this study, we identified spatially distinct cellular sources of CSF1 that regulate intestinal macrophages and contribute to antibacterial defense. Pharmacological blockade of CSF1R signaling led to macrophage depletion, and genetic ablation of CSF1 resulted in a marked reduction of these cells, whereas IL-34 deficiency alone had no significant impact. Using a *Csf1*-fate-mapping mouse model, we observed co-localization of macrophages with CSF1-expressing PDPN$^+$ fibroblasts, suggesting that fibroblasts are key niche components for macrophage maintenance. Conditional deletion of CSF1 in various cell types confirmed that fibroblast-derived CSF1 is a dominant and essential niche factor for sustaining gut macrophage populations.

In addition to fibroblasts, we identified endothelial cells as another source of CSF1 in the small intestine. Previous studies have shown that macrophages regulate vascular permeability by interacting with endothelial cells, thereby preventing infiltration of commensal bacteria and leukocytes[64,65]. In *Lyve1*$^{Cre/+}$; *Csf1*$^{fl/fl}$ mice, where *Csf1* expression is selectively deleted in endothelial cells, macrophages in the lower villus + SM region were reduced, while CD163$^+$ macrophages remained unaffected. These findings suggest that endothelial cell-derived CSF1 supports a distinct macrophage subset, separate from CD163$^+$ macrophages. Given the heterogeneity of intestinal vasculature and the long-lived nature of macrophages in the lower villus + SM[19,66], our results point to a specialized endothelial cell-macrophage niche, although its precise function remains to be defined.

In the brain, CSF1 and IL-34 exhibit spatially distinct expression patterns, with IL-34 maintaining microglia in the cortex and CSF1 supporting those in the white matter and cerebellum[67,68]. In the intestine, PDGFRα^{high} fibroblasts beneath the epithelium exhibited the highest levels of *Csf1* and uniquely expressed *Il34*, suggesting that they sustain upper villus macrophages, which are rapidly replenished by BM-derived macrophages after weaning[19]. Regarding their precursors, we observed no significant changes in Ly6C^{high} monocyte number in the blood of *Twist2*$^{Cre/+}$; *Csf1*$^{fl/fl}$ mice (Supplementary Fig. 8C), consistent with reports showing that CSF1 is dispensable for monocyte homeostasis[69–71].

In contrast, intestinal Ly6C^{high} monocytes were significantly reduced, suggesting that fibroblast-derived CSF1 is critical for monocyte recruitment to the gut and plays a non-redundant role in determining intestinal macrophage pool size. This conclusion was supported by parabiosis experiments, showing that local CSF1 is required for effective colonization of BM–derived macrophages. However, due to limitations of the model, we were unable to distinguish whether CSF1 and IL-34 act at the level of recruitment, differentiation, or both.

To evaluate the biological relevance of fibroblast-derived CSF1, we assessed host resistance to *S*. Typhimurium, an enteric pathogen that breaches the epithelial barrier and persists within macrophage phagosomes[72,73]. *Twist2*$^{Cre/+}$; *Csf1*$^{fl/fl}$ mice succumbed significantly earlier to infection and exhibited enhanced bacterial dissemination, whereas *Lyve1*$^{Cre/+}$; *Csf1*$^{fl/fl}$ mice showed normal survival. CSF1R inhibitor treatment abolished survival differences between *Twist2*$^{Cre/+}$; *Csf1*$^{fl/fl}$ and *Csf1*$^{fl/fl}$ mice, confirming that fibroblast-derived CSF1 is essential for macrophage-mediated containment. Interestingly, *Lepr*$^{Cre/+}$; *Csf1*$^{fl/fl}$ mice displayed normal survival, indicating that CSF1 from PDGFRα^{high} fibroblasts, rather than CD81^{+} LepR^{+} fibroblasts, plays a predominant role in gut-lumen defense.

Despite progress in characterizing macrophage subsets, a comprehensive anatomical and functional classification based on niche context remains incomplete. Our findings suggest that fibroblast-macrophage interactions establish spatially distinct macrophage niches. We confirmed that CD163^{+} macrophages are localized to the deep submucosal region[56] and are supported by CD81^{+} LepR^{+} fibroblasts rather than endothelial cells. As CD163 expression is induced by IL-10, a key homeostatic cytokine[54], it is likely that CD163^{+} macrophages preferentially reside in IL-10-rich environments.

CD81^{+} fibroblasts also support Lgr5^{+} intestinal epithelial stem cells by producing BMP inhibitors such as Glemlin-1[41]. CD163^{+} macrophages, which localize near crypts in the lower villus region, have similarly been implicated in stem cell support[20,21]. Recent studies show that Tim4^{+} macrophages are long-lived and largely derived from fetal progenitors[19,60,61]. The severe reduction of CD163^{+} Tim4^{+} macrophages in *Twist2*$^{Cre/+}$; *Csf1*$^{fl/fl}$ mice suggests that CD81^{+} LepR^{+} fibroblasts may contribute to epithelial stem cell maintenance by supporting this macrophage subset across developmental stages. Further investigations are required to clarify the cellular relationship between CD163^{+} Tim4^{+} macrophages and Lgr5^{+} stem cells.

Finally, our parabiosis experiments demonstrated that monocyte-derived CD163^{+} macrophages colonize the gut in a CSF1-dependent manner. Together, these findings indicate that CD81^{+} LepR^{+} fibroblasts serve as a niche for macrophages in the lower villus + SM region, particularly CD163^{+} macrophages. While their functional diversity and roles in gut immunity remain to be fully defined, their spatial localization and fibroblast dependence highlight their physiological significance.

In conclusion, our study shows that CSF1R ligands, particularly fibroblast-derived CSF1, are essential regulators of the intestinal macrophage pool and contribute to host defense against enteric pathogens. By identifying the cellular sources and spatial niches of CSF1R ligands, we provide a framework for developing niche-centered therapies in immune-mediated gastrointestinal diseases.

CRediT authorship contribution statement

Daichi Nonaka: Writing – original draft, Investigation, Conceptualization. **Soichiro Yoshida:** Investigation, Writing – original draft, Validation, Conceptualization. **Kenta Nakano:** Resources, Investigation. **Xiaojun Li:** Writing – review & editing, Investigation. **Tadashi Okamura:** Resources. **Eiji Umemoto:** Writing – review & editing, Resources. **Taisho Yamada:** Writing – review & editing. **Miyuki Watanabe:** Writing – review & editing, Funding acquisition. **Shozo Jinno:** Methodology. **Minako Ito:** Resources, Funding acquisition. **Makoto Tsuda:** Resources. **Naoto Noguchi:** Writing – review & editing. **Jean X Jiang:** Writing – review & editing, Resources, Funding acquisition. **Eriko Sumiya:** Writing – original draft, Validation, Supervision, Resources, Funding acquisition, Data curation, Formal analysis, Writing – review & editing. **Shinichiro Sawa:** Writing – review & editing, Writing – original draft, Validation, Supervision, Resources, Project administration, Methodology, Investigation, Funding acquisition, Formal analysis, Data curation, Conceptualization.

Acknowledgments

This work was supported by JSPS KAKENHI grants JP23K27428 (S. S.), JP17K15588 (E.S.), JP21K08417 (E.S.), JP22J40144 (E.S.), JP24K18471(M.W.) and JP22H05061 (M.I.). S.S. also receive support from JST Moonshot R&D (JPMJMS2025), AMED PRIME (JP19gm6310005), the Naito foundation and the Takeda Foundation. E. S was additionally supported by the Naito Foundation and the Tokyo Biochemical Research Foundation. L.X. was supported by the State Scholarship Fund of China Scholarship Council (202006370188). This work was also supported by the U.S. National Institutes of Health (RO1AG045040) and the Welch Foundation (AQ-1507) (J.X.J.). Additionally, it was supported in part by the MEXT Cooperative Research Project Program, Medical Research Center Initiative for High Depth Omics, and CURE: JPMXP1323015486 for MIB, Kyushu University. The infrastructure of Omics Science Center Secure Information Analysis System, Medical Institute of Bioregulation at Kyushu University provides the part of computational resource. We thank Ms. Yumiko Kitada, Ms. Noriko Kurisaki, Ms. Keiko Tanaka, Ms. Kimika Yoshino, and Mr. Yunosuke Sawa supported laboratory works and animal care. Ms. Akiko Yano provided administrative assistance.

Appendix A. Supplementary data

Supplementary data to this article can be found online at https://doi.org/10.1016/j.mucimm.2025.06.011.

References

1. Wynn TA, Chawla A, Pollard JW. Macrophage biology in development, homeostasis and disease. *Nature*. 2013;496:445–455.
2. Lazarov T, Juarez-Carreño S, Cox N, Geissmann F. Physiology and diseases of tissue-resident macrophages. *Nature*. 2023;618:698–707.
3. Okabe Y, Medzhitov R. Tissue biology perspective on macrophages. *Nat Immunol*. 2016;17:9–17.
4. Mass E, Nimmerjahn F, Kierdorf K, Schlitzer A. Tissue-specific macrophages: how they develop and choreograph tissue biology. *Nat Rev Immunol*. 2023;23:563–579.
5. Liu Z, et al. Fate mapping via Ms4a3-Expression history traces Monocyte-Derived cells. *Cell*. 2019;178:1509–1525.e1519.
6. Bain CC, et al. Constant replenishment from circulating monocytes maintains the macrophage pool in the intestine of adult mice. *Nat Immunol*. 2014;15:929–937.
7. Kayama H, Okumura R, Takeda K. Interaction between the Microbiota, Epithelia, and Immune Cells in the Intestine. *Annu Rev Immunol*. 2020;38:23–48.
8. Niess JH, et al. CX3CR1-mediated dendritic cell access to the intestinal lumen and bacterial clearance. *Science*. 2005;307:254–258.
9. Chieppa M, Rescigno M, Huang AY, Germain RN. Dynamic imaging of dendritic cell extension into the small bowel lumen in response to epithelial cell TLR engagement. *J Exp Med*. 2006;203:2841–2852.
10. Leonardi I, et al. CX3CR1(+) mononuclear phagocytes control immunity to intestinal fungi. *Science*. 2018;359:232–236.
11. Longman RS, et al. CX$_3$CR1^{+} mononuclear phagocytes support colitis-associated innate lymphoid cell production of IL-22. *J Exp Med*. 2014;211:1571–1583.
12. Denning TL, Wang YC, Patel SR, Williams IR, Pulendran B. Lamina propria macrophages and dendritic cells differentially induce regulatory and interleukin 17-producing T cell responses. *Nat Immunol*. 2007;8:1086–1094.
13. Seo SU, et al. Intestinal macrophages arising from CCR2(+) monocytes control pathogen infection by activating innate lymphoid cells. *Nat Commun*. 2015;6:8010.
14. Nagata S. Apoptosis and clearance of apoptotic cells. *Annu Rev Immunol*. 2018;36:489–517.
15. Zigmond E, et al. Macrophage-restricted interleukin-10 receptor deficiency, but not IL-10 deficiency, causes severe spontaneous colitis. *Immunity*. 2014;40:720–733.
16. Hegarty LM, Jones GR, Bain CC. Macrophages in intestinal homeostasis and inflammatory bowel disease. *Nat Rev Gastroenterol Hepatol*. 2023;20:538–553.
17. Harnik Y, et al. A spatial expression atlas of the adult human proximal small intestine. *Nature*. 2024;632:1101–1109.
18. Delfini M, Stakenborg N, Viola MF, Boeckxstaens G. Macrophages in the gut: Masters in multitasking. *Immunity*. 2022;55:1530–1548.

19. De Schepper S, et al. Self-Maintaining gut macrophages are essential for intestinal homeostasis. *Cell*. 2018;175:400–415.e413.
20. Sehgal A, et al. The role of CSF1R-dependent macrophages in control of the intestinal stem-cell niche. *Nat Commun*. 2018;9:1272.
21. Saha S, et al. Macrophage-derived extracellular vesicle-packaged WNTs rescue intestinal stem cells and enhance survival after radiation injury. *Nat Commun*. 2016; 7:13096.
22. van de Laar L, et al. Yolk Sac Macrophages, Fetal Liver, and Adult Monocytes can Colonize an empty Niche and develop into Functional Tissue-Resident Macrophages. *Immunity*. 2016;44:755–768.
23. Lavin Y, et al. Tissue-resident macrophage enhancer landscapes are shaped by the local microenvironment. *Cell*. 2014;159:1312–1326.
24. Gross-Vered M, et al. Defining murine monocyte differentiation into colonic and ileal macrophages. *Elife*. 2020;9.
25. Kang B, et al. Commensal microbiota drive the functional diversification of colon macrophages. *Mucosal Immunol*. 2020;13:216–229.
26. Becker S, Warren MK, Haskill S. Colony-stimulating factor-induced monocyte survival and differentiation into macrophages in serum-free cultures. *J Immunol*. 1987;139:3703–3709.
27. Pierce JH, et al. Macrophage-colony-stimulating factor (CSF-1) induces proliferation, chemotaxis, and reversible monocytic differentiation in myeloid progenitor cells transfected with the human c-fms/CSF-1 receptor cDNA. *PNAS*. 1990;87:5613–5617.
28. Lin H, et al. Discovery of a cytokine and its receptor by functional screening of the extracellular proteome. *Science*. 2008;320:807–811.
29. Dai XM, et al. Targeted disruption of the mouse colony-stimulating factor 1 receptor gene results in osteopetrosis, mononuclear phagocyte deficiency, increased primitive progenitor cell frequencies, and reproductive defects. *Blood*. 2002;99: 111–120.
30. McNamara NB, et al. Microglia regulate central nervous system myelin growth and integrity. *Nature*. 2023;613:120–129.
31. Guilliams M, Thierry GR, Bonnardel J, Bajenoff M. Establishment and Maintenance of the Macrophage Niche. *Immunity*. 2020;52:434–451.
32. Jung S, et al. Analysis of fractalkine receptor CX(3)CR1 function by targeted deletion and green fluorescent protein reporter gene insertion. *Mol Cell Biol*. 2000; 20:4106–4114.
33. Elmore MR, et al. Colony-stimulating factor 1 receptor signaling is necessary for microglia viability, unmasking a microglia progenitor cell in the adult brain. *Neuron*. 2014;82:380–397.
34. Mikkelsen HB, Thuneberg L. Op/op mice defective in production of functional colony-stimulating factor-1 lack macrophages in muscularis externa of the small intestine. *Cell Tissue Res*. 1999;295:485–493.
35. Chitu V, Stanley ER. Colony-stimulating factor-1 in immunity and inflammation. *Curr Opin Immunol*. 2006;18:39–48.
36. Dai XM, Zong XH, Sylvestre V, Stanley ER. Incomplete restoration of colony-stimulating factor 1 (CSF-1) function in CSF-1-deficient Csf1op/Csf1op mice by transgenic expression of cell surface CSF-1. *Blood*. 2004;103:1114–1123.
37. Schönig K, Schwenk F, Rajewsky K, Bujard H. Stringent doxycycline dependent control of CRE recombinase in vivo. *Nucleic Acids Res*. 2002;30:e134.
38. Madisen L, et al. A robust and high-throughput Cre reporting and characterization system for the whole mouse brain. *Nat Neurosci*. 2010;13:133–140.
39. Kinchen J, et al. Structural Remodeling of the Human Colonic Mesenchyme in Inflammatory Bowel Disease. *Cell*. 2018;175:372–386.e317.
40. McCarthy N, Kraiczy J, Shivdasani RA. Cellular and molecular architecture of the intestinal stem cell niche. *Nat Cell Biol*. 2020;22:1033–1041.
41. McCarthy N, et al. Distinct Mesenchymal Cell Populations Generate the Essential Intestinal BMP Signaling Gradient. *Cell Stem Cell*. 2020;26:391–402.e395.
42. Roulis M, et al. Paracrine orchestration of intestinal tumorigenesis by a mesenchymal niche. *Nature*. 2020;580:524–529.
43. Kim JE, et al. Single cell and genetic analyses reveal conserved populations and signaling mechanisms of gastrointestinal stromal niches. *Nat Commun*. 2020;11:334.
44. Pærregaard SI, et al. The small and large intestine contain related mesenchymal subsets that derive from embryonic Gli1(+) precursors. *Nat Commun*. 2023;14:2307.
45. Hong SP, et al. Distinct fibroblast subsets regulate lacteal integrity through YAP/ TAZ-induced VEGF-C in intestinal villi. *Nat Commun*. 2020;11:4102.
46. Shoshkes-Carmel M, et al. Subepithelial telocytes are an important source of Wnts that supports intestinal crypts. *Nature*. 2018;557:242–246.
47. Kraiczy J, et al. Graded BMP signaling within intestinal crypt architecture directs self-organization of the Wnt-secreting stem cell niche. *Cell Stem Cell*. 2023;30: 433–449.e438.
48. Šošić D, Richardson JA, Yu K, Ornitz DM, Olson EN. Twist regulates cytokine gene expression through a negative feedback loop that represses NF-kappaB activity. *Cell*. 2003;112:169–180.
49. Harris SE, et al. Meox2Cre-mediated disruption of CSF-1 leads to osteopetrosis and osteocyte defects. *Bone*. 2012;50:42–53.
50. Pham TH, et al. Lymphatic endothelial cell sphingosine kinase activity is required for lymphocyte egress and lymphatic patterning. *J Exp Med*. 2010;207:17–27.
51. Lee LK, et al. LYVE1 Marks the Divergence of Yolk Sac Definitive Hemogenic Endothelium from the Primitive Erythroid Lineage. *Cell Rep*. 2016;17:2286–2298.
52. Zhang N, et al. LYVE1+ macrophages of murine peritoneal mesothelium promote omentum-independent ovarian tumor growth. *J Exp Med*. 2021;218.
53. Etzerodt A, Moestrup SK. CD163 and inflammation: biological, diagnostic, and therapeutic aspects. *Antioxid Redox Signal*. 2013;18:2352–2363.
54. Kayama H, et al. Intestinal CX3C chemokine receptor 1(high) (CX3CR1(high)) myeloid cells prevent T-cell-dependent colitis. *PNAS*. 2012;109:5010–5015.
55. Leshan RL, Björnholm M, Münzberg H, Myers Jr MG. Leptin receptor signaling and action in the central nervous system. *Obesity (Silver Spring)*. 2006;14(Suppl 5): 208s–s212.
56. Prise, I. E. et al. CD163 and Tim-4 identify resident intestinal macrophages across sub-tissular regions that are spatially regulated by TGF-β. *bioRxiv*, 2023.2008.2021.553672 (2023).
57. Bain CC, Schridde A. Origin, Differentiation, and Function of Intestinal Macrophages. *Front Immunol*. 2018;9:2733.
58. Ginhoux F, Guilliams M. Tissue-Resident Macrophage Ontogeny and Homeostasis. *Immunity*. 2016;44:439–449.
59. Bonnardel J, et al. Stellate Cells, Hepatocytes, and Endothelial Cells Imprint the Kupffer Cell Identity on Monocytes Colonizing the Liver Macrophage Niche. *Immunity*. 2019;51:638–654.e639.
60. Shaw TN, et al. Tissue-resident macrophages in the intestine are long lived and defined by Tim-4 and CD4 expression. *J Exp Med*. 2018;215:1507–1518.
61. Chiaranunt P, et al. Microbial energy metabolism fuels an intestinal macrophage niche in solitary isolated lymphoid tissues through purinergic signaling. *Sci Immunol*. 2023;8, eabq4573.
62. Barthel M, et al. Pretreatment of mice with streptomycin provides a Salmonella enterica serovar Typhimurium colitis model that allows analysis of both pathogen and host. *Infect Immun*. 2003;71:2839–2858.
63. Park MD, Silvin A, Ginhoux F, Merad M. Macrophages in health and disease. *Cell*. 2022;185:4259–4279.
64. Chakarov S, et al. Two distinct interstitial macrophage populations coexist across tissues in specific subtissular niches. *Science*. 2019;363.
65. Honda M, et al. Perivascular localization of macrophages in the intestinal mucosa is regulated by Nr4a1 and the microbiome. *Nat Commun*. 2020;11:1329.
66. Drokhlyansky E, et al. The Human and Mouse Enteric nervous System at Single-Cell Resolution. *Cell*. 2020;182:1606–1622.e1623.
67. Easley-Neal C, Foreman O, Sharma N, Zarrin AA, Weimer RM. CSF1R Ligands IL-34 and CSF1 are Differentially Required for Microglia Development and Maintenance in White and Gray Matter Brain Regions. *Front Immunol*. 2019;10:2199.
68. Kana V, et al. CSF-1 controls cerebellar microglia and is required for motor function and social interaction. *J Exp Med*. 2019;216:2265–2281.
69. Zhang J, et al. In situ mapping identifies distinct vascular niches for myelopoiesis. *Nature*. 2021;590:457–462.
70. Emoto T, et al. Colony stimulating factor-1 producing endothelial cells and mesenchymal stromal cells maintain monocytes within a perivascular bone marrow niche. *Immunity*. 2022;55:862–878.e868.
71. Thierry GR, et al. Non-classical monocytes scavenge the growth factor CSF1 from endothelial cells in the peripheral vascular tree to ensure survival and homeostasis. *Immunity*. 2024;57:2108–2121.e2106.
72. Jones BD. Host responses to pathogenic Salmonella infection. *Genes Dev*. 1997;11: 679–687.
73. Muller PA, et al. Crosstalk between muscularis macrophages and enteric neurons regulates gastrointestinal motility. *Cell*. 2014;158:300–313.